NiFe$_2$O$_4$ Nanoparticles Dispersed in an Aerogel Silica Matrix: An X-ray Absorption Study

Daniela Carta, Danilo Loche, Gavin Mountjoy,[1] Gabriele Navarra, and Anna Corrias*

Dipartimento di Scienze Chimiche and INSTM, Università di Cagliari, S.P. Monserrato-Sestu Km 0.700, I-09042 Monserrato, Cagliari, Italy

The formation of NiFe$_2$O$_4$ nanoparticles dispersed in an aerogel silica matrix was investigated as a function of calcination temperature by X-ray absorption fine structure and X-ray absorption near edge structure at both the Fe and Ni K-edges. In particular, nanocomposite aerogels containing a relative NiFe$_2$O$_4$ amount of 10 wt % and calcined at 450, 750 (1 h and 20 h), and 900 °C were studied. A quantitative determination of the relative occupancy of iron and nickel cations in the octahedral and tetrahedral sites of the spinel structure was obtained. It has been found that nickel ferrite prepared by sol−gel has the classical inverted spinel structure found in bulk materials with nickel(II) cations fully occupying the octahedra sites and iron(III) equally distributed between octahedra and tetrahedra sites.

I. Introduction

Transition metals ferrites, MFe$_2$O$_4$ (where M = Co, Ni, Mn, Mg, Zn, etc.) have been of great interest in recent years for their remarkable magnetic, optical, and electrical properties. In particular, nanocrystalline transition metal ferrites have been an important subject of research as they exhibit unique properties, different from those of bulk materials. For example, the magnetic properties are particularly affected at the nanometric level, because when the particle size decreases down to the nanometric range, each particle can behave as a single magnetic domain. Nanocrystalline transition metals ferrites find applications in magnetic storage devices,[1] site-specific drug delivery,[2] and photomagnetic materials.[3]

Nickel ferrite nanoparticles (NiFe$_2$O$_4$) have been widely used in electronic devices because of the large permeability at high frequency and high electrical resistivity.[4] Recently, they have been used as magnetic resonance imaging contrast agents,[5] as anode material for lithium ion batteries,[6] and as catalyst for coupling reactions of aromatic halide derivatives when surface-modified with Pd.[7]

Nanocrystalline nickel ferrite can be prepared by hydrothermal route,[8] ball-milling,[9] coprecipitation,[10] combustion reaction,[11] and reverse micelles technique.[12] However, nonsupported nickel ferrite nanoparticles may aggregate and grow, and this would have a negative effect on the magnetic and catalytic properties. The homogeneous dispersion of the nanoparticles in an amorphous matrix, giving rise to magnetic nanocomposite materials, could provide a solution to this problem. Magnetic nanocomposites have peculiar and tuneable catalytic, electric, and magnetic properties, different from those of bulk materials, that depend not only on particle size and distribution of the nanocrystals, but also on the morphology and porosity of the matrix and on the interaction between the nanocrystals and the matrix.

The sol−gel route has been proven to be successful in the synthesis of composites of nickel ferrite nanoparticles dispersed in a silica matrix.[13−16] In fact, the formation of the nanoparticles

in the starting sol allows a good control of composition, purity, homogeneity, particle sizes, and distribution. Most of the works published so far follow the traditional sol−gel route, where the drying of the gels is performed by thermal treatment (xerogels); this causes cracking of the gels and collapse of the porous structure. However, the preservation of the porous structure is quite important, especially for avoiding interactions between the magnetic nanoparticles and for catalytic applications where the surface area plays a very important role. In the present work, we have studied nanocomposites containing NiFe$_2$O$_4$ dispersed in a very highly porous silica host obtained through supercritical drying of the gel. This special drying technique avoids the capillary forces at the liquid/vapor interface responsible for formation of cracks and collapsing of the porous structure. Therefore, the products after drying (aerogels) present low densities, high porosities, and high surface areas.

The samples studied in this work are aerogels containing 10 wt % NiFe$_2$O$_4$/(NiFe$_2$O$_4$ + SiO$_2$) calcined in air at increasing temperatures (450, 750 for 1 h and 20 h, and 900 °C). X-ray absorption techniques, extended X-ray absorption fine structure (EXAFS) and X-ray absorption near edge structure (XANES), were used to study the evolution of the aerogel systems with calcination temperature. EXAFS and XANES have shown to be powerful tools for the structural study of nanocomposites of metal oxides, alloys, and ferrite nanoparticles dispersed in an amorphous matrix prepared by the sol−gel process.[17−23] X-ray absorption spectroscopy[24] is an ideal probe for studying multicomponent dilute and disordered materials, being element specific and sensitive to the local structure. EXAFS gives information about bond distances and coordination numbers of shells surrounding the absorbing atom; XANES gives information on oxidation state and site-symmetry of the absorbing atom.

Another very important aspect in the study of the final nanocomposite aerogels is the determination of the cations distribution in the NiFe$_2$O$_4$ ferrite nanoparticles. In the structure of ferrites, bivalent and trivalent cations reside on tetrahedral and octahedral interstitial sites available in the close packing of oxygen anions.[25−27] The cation distribution is defined by the inversion parameter *i*, which indicates the fraction of bivalent cations in octahedral sites. An accurate estimation of the inversion degree is essential in order to understand the properties

* To whom correspondence should be addressed. E-mail: corrias@unica.it.
[1] Permanent address: School of Physical Sciences, Ingram Building, University of Kent, Canterbury, CT2 7NH, UK.

of ferrites since different cation distributions crucially influences the catalytic, magnetic, and electronic properties.

X-ray and neutron diffraction[28] and Mössbauer spectroscopy[29] have been used for the determination of the cation distribution. However, the usefulness of XRD is limited by the similar scattering factors of Ni and Fe and by the nanodimension of the particles that broadens the peaks. Mössbauer spectroscopy is effective in determining the environment of Fe ions but does not provide information on the Ni cations and is not very effective for dilute samples.[30] In this work, we have used EXAFS spectroscopy at the Fe and Ni K-edge, which seems the most promising technique to study the cation site distribution of nickel ferrite nanoparticles dispersed in an amorphous matrix, since it allows one to separately and independently study the environment around the Fe and Ni ions.

II. Experimental Section

A. Sample Preparation. The samples were prepared by sol−gel process using tetraethoxysilane (($Si(OC_2H_5)_4$, Aldrich 98%, TEOS) as a precursor for silica, iron(III) and nickel(II) nitrates ($Fe(NO_3)_3 \cdot 9H_2O$, Aldrich, 98%, and $Ni(NO_3)_2 \cdot 6H_2O$, Aldrich, 99.999%) as precursors for the nickel ferrite phases and absolute ethanol (EtOH, Fluka, 99%) as mutual solvent. The precursors were added in such a way to obtain nanocomposites containing a nominal ratio of 10 wt % $NiFe_2O_4/(NiFe_2O_4 + SiO_2)$. The ethanolic solution of the metal salts was added into the prehydrolyzed TEOS under acidic catalysis. A hydroalcoholic solution of urea (NH_2CONH_2, Aldrich, >99.0%) was then added under reflux for 2 h at 85 °C as basic gelation agent. The sols were left in a closed container at 40 °C; gelation occurred in less than 1 day. The alcogels were submitted to high-temperature supercritical drying in an autoclave (Parr, 300 cm^3). The autoclave containing the sample and an appropriate amount of ethanol was flushed with N_2, closed, and heated until reaching 330 °C and 70 atm, conditions when the solvent is in the supercritical state. The autoclave was then vented, and highly porous aerogel samples were obtained. The samples were calcined at 450, 750 (1 h and 20 h), and 900 °C. The aerogels will be hereafter called AFeNi_XXX_Y, where XXX refers to the calcination temperature and Y refers to the calcinations time. An aerogel containing only nickel was also prepared with the same procedure and calcined at 450 °C, and it will be hereafter called ANi_450. Nickel silicate hydroxide to be used as a reference compound was synthesized using the route described in ref 31. Briefly, 8 mL of a 0.1 M solution of Na_2SiO_3 (Alfa Aesar) were added to 2 mL of a solution 0.3 M anhydrous $NiCl_2$ (Alfa Aesar, 98%) in the presence of 0.4 mL of a 1 M solution of HCl. The precipitate obtained was washed with distilled water. After being dispersed in 500 mL of distilled water, the precipitate was left in a covered beaker at 75 °C for 2 weeks and then filtered and dried in an oven at 40 °C. Commercial $NiFe_2O_4$ was also used as a reference (Aldrich >98%).

B. X-Ray Diffraction (XRD) Data Collection. XRD spectra were recorded on a X3000 Seifert diffractometer equipped with a graphite monochromator on the diffracted beam. The scans were collected within the range of 10−70 degrees (2θ) using Cu Kα radiation.

C. X-ray Absorption Data Collection (XANES and EX-AFS). EXAFS and XANES data were collected in transmission mode at beamline 11.1 (XAFS) at the ELETTRA synchrotron (Trieste, Italy). Spectra at the Fe (7112 eV) and Ni (8333 eV) K-edges were acquired at room temperature using a Si(111) monochromator. Data were collected on samples calcined at 450, 750 (1 h and 20 h), and 900 °C. Data were also collected on commercial $NiFe_2O_4$ and on a nickel silicate hydroxide as

reference materials. Samples with a suitable and highly uniform optical thickness were prepared from powders. In the case of the reference samples, the powders were dispersed in an inert solvent and then filtered onto polyethylene supports. The aerogel samples were pressed into a cardboard frame with mylar windows without the need of using any diluent, the aerogels being very easy to compress due to their very low apparent density.

D. EXAFS Data Analysis. The program Viper was used to sum the data, identify the beginning of the absorption edge (E_0), fit pre- and postedge backgrounds, and hance to obtain the normalized absorbance (χ) as a function of the modulus of the photoelectron wavevector (k).[32] The modular package DL_EXCURV,[33] based on the EXCURV98 code, was used in the final stage of data processing to model the experimental $\chi(k)$ in order to extract structural information. This code uses fast curved wave theory[34] and calculates ab initio the effective curved wave backscattering amplitude of the scatterer, the phase shift due to the absorbing atom potential, the phase shift due to the scatterer, and the mean free path of the photoelectron.[35,36] In DL_EXCURV, the k-independent parameter AFAC (many-body amplitude reduction factor) was determined to be 0.9 from fitting to the reference samples. The parameter EF, which is a correction to E_0, was free to vary in all fittings. A nonlinear least-squares fitting in k-space with a k^3 weighting of the total experimental EXAFS spectra, to emphasize the high-energy part of the spectrum, allowed us to obtain the structural parameters, including the degree of inversion of the nickel ferrite (i), which corresponds to the fraction of Ni^{2+} ions in octahedral sites. This is possible because the EXCURV98 code, as reported in the manual,[37] allows one to introduce different sites (clusters) containing the excited atom and to fit the occupancy of each sites. The fitting was carried out using the k range 2.5−12 Å^{-1}. The errors in the fit parameters were obtained from the 95% confidence level,[38] as calculated in EXCURV98. The number of fitted parameters was always less than the number of statistically independent data points, as estimated in the standard way.[38]

The quality of the fit was judged from the normalized sum of residuals (eq 1).

$$R\text{-factor} = \frac{\sum_n k_n^3 |\chi_{\text{expt}}(k_n) - \chi_{\text{fit}}(k_n)|}{\sum_n k_n^3 |\chi_{\text{expt}}(k_n)|} \times 100 \quad (1)$$

R-factors were calculated on the experimental $k^3\chi(k)$, and *R-factors were calculated on the Fourier-filtered $k^3\chi(k)$. The Fourier-filtered $k^3\chi(k)$ is obtained by inverse transforming only the part of the Fourier transform (FT) corresponding to the shells that were fitted. *R-factor is more meaningful in stating the goodness of the fit since the backtransforms exclude contributions that were not included in the fitting (i.e., contributions at low R due to imperfect background removal and contributions at high R due to large distance shells). Reasonable EXAFS fits of single shells typically have R-factor values around 20%; however, when the fit is performed on the total EXAFS spectra, higher R-factor values can still correspond to good fits, especially if the fit is not extended to peaks at high R.

E. XANES Data Analysis. The XANES spectra were processed in the usual way to obtain normalized absorbance.[39] XANES at the K-edge involves the excitation of a 1s photoelectron into low-lying empty states at the central atom with p-type symmetry. The K-edge XANES spectra in transition metals has a gradually sloping main absorption edge, with a pronounced step on the low energy side, a rounded main
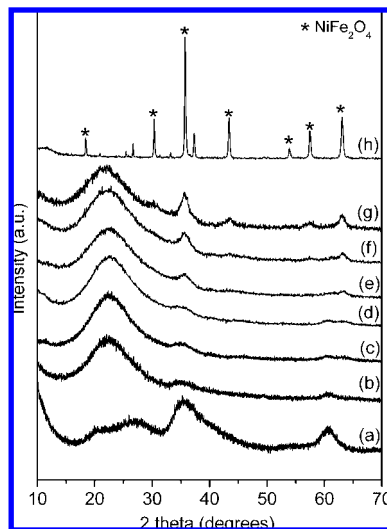
NiFe$_2$O$_4$ Nanoparticles in an Aerogel Silica Matrix

J. Phys. Chem. C, Vol. 112, No. 40, 2008 **15625**

Figure 1. XRD patterns of Ni$_3$Si$_2$O$_5$(OH)$_4$ (a), ANi_450 (b), AFeNi_ae (c), AFeNi_450 (d), AFeNi_750_1h (e), AFeNi_750_20h (f), AFe-Ni_900 (g), and NiFe$_2$O$_4$ (h).

Figure 2. $k^3\chi(k)$ spectra at the Fe K-edge (A) and Ni K-edge (B) from experiment (—) and fit results ($\cdots$). (A): AFeNi_ae (a), AFeNi_450 (b), AFeNi_750_1h (c), AFeNi_750_20h (d), AFeNi_900 (e), and NiFe$_2$O$_4$ (f). (B): Ni$_3$Si$_2$O$_5$(OH)$_4$ (a), ANi_450 (b), AFeNi_ae (c), AFeNi_450 (d), AFeNi_750_1h (e), AFeNi_750_20h (f), AFeNi_900 (g), and NiFe$_2$O$_4$ (h).

absorption edge peak, and approximately constant intensity following the edge. In contrast, transition metal oxides have a sharply rising main absorption edge, with main absorption edge peak(s) of high intensity, and a notable drop in intensity after the main absorption edge peak. In addition, oxides may show a small pre-edge peak if the excited atom site has a lack of centrosymmetry. In both metals and oxides, oscillations in intensity occurring up to approximately 30 eV beyond the absorption edge are due to strong multiple-scattering or shape resonance around the excited atom site. The XANES spectra have been analyzed using the "fingerprint" method, by comparing spectra from samples with those from reference compounds.

III. Results

A. XRD. The XRD patterns of the aerogels after extraction and after calcination at 450, 750 (1 h and 20 h), and 900 °C, along with the aerogel containing only Ni calcined at 450 °C, nickel silicate hydroxide, and commercial nickel ferrite are presented in Figure 1. In the pattern of nickel silicate hydroxide, two broad reflexions at $2\theta \approx 35°$ and $2\theta \approx 60°$ are observed. These peaks are typical of layered phyllosilicate-like structures. In particular, they are typical of the structure of Ni$_3$Si$_2$O$_5$(OH)$_4$.[40] In the patterns of ANi_450, AFeNi_ae, and AFeNi_450, the same two broad and weak reflexions at $2\theta \approx 35°$ and $2\theta \approx 60°$ are detectable along with the broad halo around $2\theta \approx 20°$ due to the silica matrix. After calcination at 750 °C for 1 h, broad peaks corresponding to the most intense nickel ferrite phase reflexions[41] appear superimposed on the amorphous silica halo. The peaks become more intense and sharper with the increase of calcination time and temperature. The XRD pattern of the commercial nickel ferrite shows sharp peaks corresponding to all the reflexions of NiFe$_2$O$_4$, indicating a larger size of crystal domains compared to the aerogels. In addition to these peaks, some unidentified peaks are observed, due to the presence of some impurities.

B. EXAFS. In Figure 2A, the EXAFS spectra at the Fe K-edge for the AFeNi_ae, AFeNi_450, AFeNi_750_1h, AFeNi_750_20h, and AFeNi_900 samples are shown along with those of commercial NiFe$_2$O$_4$. The oscillations of AFeNi_ae and AFeNi_450 are quite weak and do not appear up to high k, unlike those observed for AFeNi_900 and NiFe$_2$O$_4$. The oscillations are very similar to those of ferrihydrite, a poorly

crystallized phase of iron(III) oxyhydroxide, whose EXAFS spectrum is reported in ref 22. Therefore, Fe is present as ferrihdydrite in both AFeNi_ae and AFeNi_450. With increasing calcination temperature from 450 to 900 °C, the oscillation frequencies of the nanocomposites become progressively more similar to those of NiFe$_2$O$_4$. In particular, the oscillations of AFeNi_750_1h seem to arise from a combination of the phases present in AFeNi_450 and AFeNi_750_20h. Finally, AFeNi_900 shows oscillations typical of a well-crystallized compound (up to high k) and very similar to those of NiFe$_2$O$_4$, even if the amplitude of the oscillations is smaller.

In Figure 2B, the EXAFS spectra at the Ni K-edge for AFeNi_ae, AFeNi_450, AFeNi_750_1h, AFeNi_750_20h, and AFeNi_900 samples are shown, along with those of the ANi_450 aerogel (containing only nickel) and the reference compounds Ni$_3$Si$_2$O$_5$(OH)$_4$ and NiFe$_2$O$_4$.

The oscillations of AFeNi_ae and AFeNi_450 seem to be very similar to those of ANi_450, indicating that the nickel is present as a separate nickel phase in the aerogel after extraction and after calcination at 450 °C. Moreover, both frequencies and amplitudes of the oscillations in ANi_450 seem very similar to those of the reference compound Ni$_3$Si$_2$O$_5$(OH)$_4$. Therefore, there is a strong indication that Ni is present in the form of nickel silicate hydroxide in the aerogels before thermal treatments at high temperature are performed. However, the oscillations in AFeNi_450 are less intense than those of ANi_450, suggesting the presence of a more disordered nickel silicate hydroxide phase. With increasing calcination temperature, the oscillations of the nanocomposites become more similar to those of NiFe$_2$O$_4$, as already observed at the Fe K-edge. In particular, AFeNi_900 shows very similar oscillations of NiFe$_2$O$_4$ with lower amplitudes, whereas AFeNi_750_1h seems to correspond to an intermediate step between AFeNi_450 and AFeNi_750_20h.

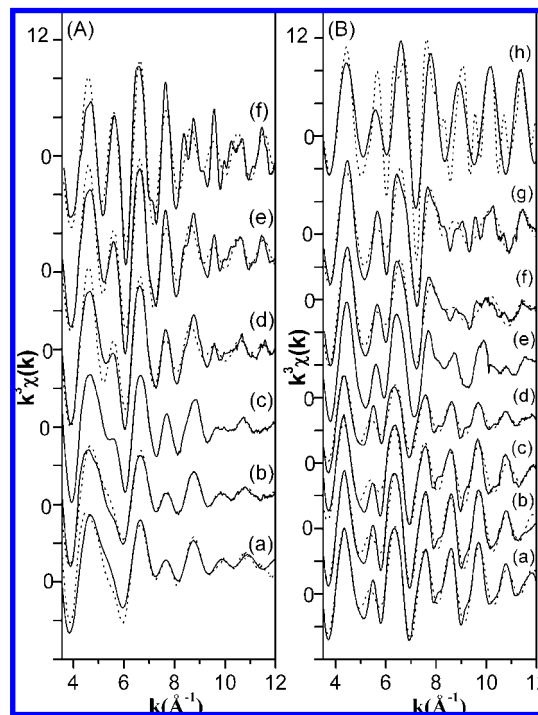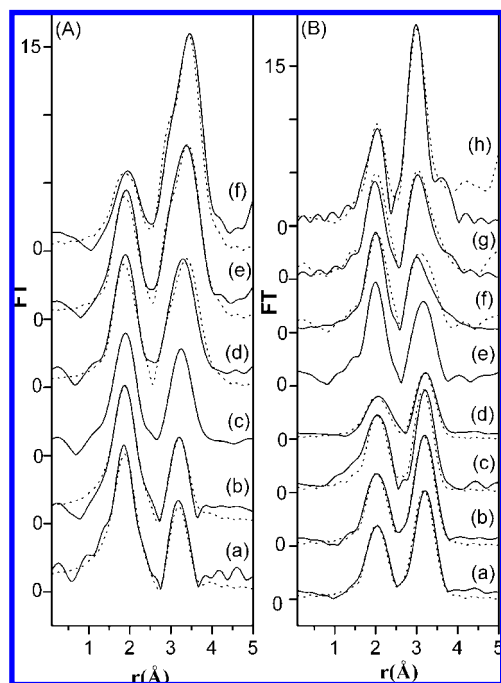**Figure 3.** Fourier transforms of $k^3\chi(k)$ spectra at the Fe K-edge (A) and Ni K-edge (B) from experiment (—) and fit results (···). (A): AFeNi_ae (a), AFeNi_450 (b), AFeNi_750_1h (c), AFeNi_750_20h (d), AFeNi_900 (e), and NiFe$_2$O$_4$ (f). (B): Ni$_3$Si$_2$O$_5$(OH)$_4$ (a), ANi_450 (b), AFeNi_ae (c), AFeNi_450 (d), AFeNi_750_1h (e), AFeNi_750_20h (f), AFeNi_900 (g), and NiFe$_2$O$_4$ (h).
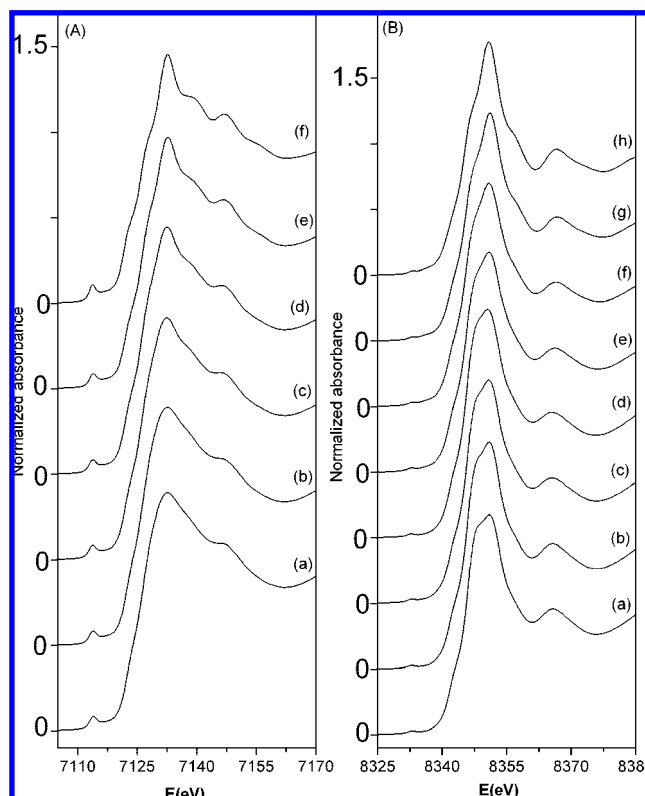

Figure 4. XANES spectra at the Fe K-edge (A) and Ni K-edge (B) from experiment (—) and fit results (···). (A): AFeNi_ae (a), AFeNi_450 (b), AFeNi_750_1h (c), AFeNi_750_20h (d), AFeNi_900 (e), and NiFe$_2$O$_4$ (f). (B): Ni$_3$Si$_2$O$_5$(OH)$_4$ (a), ANi_450 (b), AFeNi_ae (c), AFeNi_450 (d), AFeNi_750_1h (e), AFeNi_750_20h (f), AFeNi_900 (g), and NiFe$_2$O$_4$ (h).

FTs at the Fe and Ni K-edge for the same samples are reported in Figure 3, panels A and B, respectively. The trends observed in the $k^3\chi(k)$ spectra are confirmed by the analysis of the FTs. Peaks beyond the first shell are detectable at both edges. At the Fe K-edge, the FTs of AFeNi_ae and AFeNi_450 are very similar to the FT of ferrihydrite,[22] confirming the presence of ferrihydrite in the aerogels after extraction and after calcination at 450 °C. The small and broad second shell peak is consistent with the poor crystallinity of ferrihydrite. The second peak in the FTs become more prominent with the increase of the calcination temperature, indicating the formation of a phase with a well-defined structure.

At the Ni K-edge, the FTs of ANi_450 and AFeNi_ae are very similar to the FT of Ni$_3$Si$_2$O$_5$(OH)$_4$. They show, in addition to a first shell, a well-defined and intense second shell, corresponding to a single Ni–Ni correlation in a quite symmetric environment. The FT of AFeNi_450 shows the same peaks present in ANi_450 and AFeNi_ae, which are, although broader and weaker, indicative of a more disordered nickel silicate hydroxide structure, in agreement with the less intense amplitude of the EXAFS oscillations. After the thermal treatment at 750 °C for 20 h, the second shell is shifted at lower r values, in agreement with the formation of some NiFe$_2$O$_4$. AFeNi_750_1h seems to be an intermediate step in the evolution of the AFeNi_450 sample, which contains a separate nickel phase, to the AFeNi_750_20h, which contains NiFe$_2$O$_4$. With increasing calcination temperature, the FTs become more similar to that of commercial NiFe$_2$O$_4$, at both Fe and Ni edge. However, it has to be noted that the FTs of AFeNi_900 at both edges show some differences compared to that of commercial NiFe$_2$O$_4$. This could be ascribed to the presence of some impurities in commercial NiFe$_2$O$_4$, as shown by XRD analysis.

The evolution of the nanocomposite, as shown by the results at both the Fe and Ni edges, goes from a system containing iron and nickel ions in two separate phases, ferrihydrite and nickel silicate hydroxide (present up to calcination at 450 °C), to a nickel ferrite phase that begins to form at 750 °C, and it is fully developed at 900 °C.

C. XANES. The XANES spectra are shown in Figure 4, panels A and B, at the Fe and Ni K-edges respectively. For all the samples, the position of the main peak at the Fe edge is typical of iron in the +3 oxidation state, whereas at the Ni edge, the peak positions are typical of Ni in the +2 oxidation state. At the Fe edge, the absorptions profiles of AFeNi_ae and AFeNi_450 are very similar to that of ferridhydrite.[22] At the Ni edge, the absorption of AFeNi_ae, AFeNi_450, and ANi_450 are very similar to that of Ni$_3$Si$_2$O$_5$(OH)$_4$. This confirms that AFeNi_ae and AFeNi_450 contain separated iron (ferrihydrite) and nickel (nickel silicate hydroxide) phases. However, AFeNi_450 has a slightly different prepeak and main edge shape than nickel silicate hydroxide.

At both edges, the heat treatment causes the spectra to become more similar to NiFe$_2$O$_4$. AFeNi_750_20 h is similar to both AFeNi_900 and NiFe$_2$O$_4$, whereas AFeNi_750_1h seems to be an intermediate step, in agreement with the EXAFS results.

D. EXAFS Fitting. *1. Reference Compounds. NiFe$_2$O$_4$ Standard.* EXAFS data of commercial NiFe$_2$O$_4$ has been fitted considering as starting values for distances and coordination numbers the parameters found in literature.[42] The starting value for the inversion degree was set to 1, which corresponds to a totally inverted spinel structure. According to this distribution, the iron cations are equally distributed between octahedral and tetrahedral sites, and all the nickel cations occupy octahedral sites.

NiFe$_2$O$_4$ Nanoparticles in an Aerogel Silica Matrix

J. Phys. Chem. C, Vol. 112, No. 40, 2008 **15627**

TABLE 1: Interatomic Distances (R), Coordination Numbers (N), Debye−Waller Factors (σ), and Fractions of Cations in Sites A (x_A) and B (x_B)[a]

	Fe K-edge				Ni K-edge		
	R (Å)	N	$2\sigma^2$		R (Å)	N	$2\sigma^2$
$x_B = 0.50(3)$				$x_B = 1.00(2)$			
O	2.04(1)	6.0	0.025(1)	O	2.04(1)	6.0	0.016(4)
Fe	2.95(1)	6.0	0.018(2)	Ni	2.94(1)	6.0	0.006(1)
Fe	3.46(1)	6.0	0.017(2)	Ni	3.46(1)	6.0	0.019(3)
O	3.52(5)	2.0	0.032(5)	O	3.52(5)	2.0	0.020(4)
O	3.64(5)	6.0	0.031(5)	O	3.64(3)	6.0	0.018(8)
$x_A = 0.50(3)$							
O	1.89(1)	4.0	0.022(2)				
Fe	3.46(1)	12.0	0.018(1)				
O	3.47(3)	12.0	0.031(5)				
Fe	3.61(3)	4.0	0.019(1)				
	R-factor $= 39\%$			R-factor $= 54\%$			
	*R-factor $= 22\%$			*R-factor $= 35\%$			

[a] Obtained by fitting the experimental EXAFS spectra of commercial NiFe$_2$O$_4$ at the Fe and Ni K-edge.

Therefore, the fitting of nickel ferrite was done considering two clusters of atoms, one having the absorbing atom (Fe or Ni) in tetrahedral sites (Fe$_A$ and Ni$_A$) and the other one having the absorbing atom (Fe or Ni) in octahedral sites (Fe$_B$ and Ni$_B$). The distribution of the absorbing atom (Fe or Ni) between tetrahedral (A) sites and octahedral (B) sites was specified by a single variable parameter, the occupancy of (B) sites, x_B, since the occupancy of (A) sites is consequentially determined from $x_A = 1 - x_B$. The fraction of Ni^{2+} cations in octahedral sites x_B(Ni^{2+}) exactly corresponds to the inversion parameter i. Finally, the stoichiometry of spinel ferrites requires that the fraction of Fe^{3+} in (B) sites must satisfy the requirement x_B(Fe^{3+}) $= (2 - x_B$(Ni^{2+}))/2.

Because of the similar backscattering amplitudes of Fe and Ni, only Fe backscatterers are considered at Fe edge and only Ni backscatterers at the Ni edge in order to simplify the fitting. The fitting was performed keeping N_i fixed for all the shells around the excited atom, allowing small variations of R_i (within the experimental error), and $2\sigma_i^2$, EF, and the occupancy of (B) sites x_B(Ni^{2+}), that is, the inversion parameter i, were left free to vary.

The results of the fitting of commercial NiFe$_2$O$_4$ are reported in Figures 2A/3A and 2B/3B at the Fe and Ni K-edge, respectively. The best fitting parameters are reported in Table 1.

At the Fe edge, the first peak near 2 Å appears to be due to the overlapping of the contribution from two Fe−O bond distances, Fe$_A$−O (1.89 Å) and Fe$_B$−O (2.04 Å), corresponding to the tetrahedral sites and the octahedral sites, respectively. The broad peak in the region 3−4 Å is due to a series of contributions from the Fe$_A$−Fe$_A$, Fe$_A$−Fe$_B$, Fe$_B$−Fe$_B$, Fe$_B$−O, and Fe$_A$−O.

At the Ni edge, the first peak arises from the Ni$_B$−O (2.04 Å) distance due to octahedrally coordinated Ni, and the second peak, around 3−4 Å, corresponds to Ni$_B$−Ni$_B$ and Ni$_B$−O contributions.

The results of the fitting of the inversion degree at both Fe and Ni edge confirm a totally inverted spinel structure with all Ni^{2+} in octahedral sites and Fe^{2+} equally distributed between octahedral and tetrahedral sites.

The relatively high values of the R parameter could be ascribed to the presence of some impurities, as evidenced by XRD analysis, which can affect the quality of the fitting.

Ni$_3$Si$_2$O$_5$(OH)$_4$. The fitting results of the EXAFS spectra and the corresponding FTs at the Ni K-edge for the reference compound Ni$_3$Si$_2$O$_5$(OH)$_4$ are reported in Figure 2B and 3B, respectively. The best fitting parameters at the Ni K-edge are reported in Table 2. The first peak corresponds to the first Ni−O shell at a distance of 2.07 Å coordinating 6 oxygens. The second peak is due to the overlapping of two contributions, a shell of 6 nickel atoms at a Ni−Ni distance of 3.07 Å and a shell of 4 silicon atoms at a Ni−Si distance of 3.26 Å. Distance and coordination parameters found at Ni edges are typical of the Ni$_3$Si$_2$O$_5$(OH)$_4$ clay-like system.[43]

2. Aerogels after Extraction and Aerogels Calcined at 450 °C. The results of the fitting of AFeNi_ae and AFeNi_450 at the Fe edge are reported in Figures 2A and 3A. The best-fit parameters are reported in Table 3. The EXAFS oscillations of all aerogels are very similar to those of ferrihydrite, reported in ref 22. Therefore, the same parameters were used for the fitting, that is, one shell of O and three shells of Fe.

The results of the fitting of ANi_450, AFeNi_ae, and AFeNi_450 at the Ni edge are reported in Figures 2B and 3B. The best fit parameters are reported in Table 2. The EXAFS oscillations of the three aerogels are very similar to those of Ni$_3$Si$_2$O$_5$(OH)$_4$. Therefore, the same parameters were used for the fitting, that is, one shell of O, one shell of Ni, and one shell of Si. The Debye−Waller factor obtained for the fitting of ANi_450 is similar to that of Ni$_3$Si$_2$O$_5$(OH)$_4$, indicating a quite ordered structure for the aerogel containing only nickel. The Debye−Waller factors for Ni−O and Ni−Ni distances of AFeNi_450 are higher than those of AFeNi_ae, indicating a more-disordered structure, in agreement with qualitative EXAFS analysis.

3. Aerogels Calcined at 750 and 900 °C. The results of the fitting of the EXAFS oscillations for AFeNi_750_20h and AFeNi_900 are shown in Figure 2, panels A and B, and the corresponding FTs are shown in Figure 3, panels A and B, at the Fe and Ni edge, respectively. The refined parameters are reported in Table 4. The fitting for all aerogels was obtained using the same R and N values used for the commercial NiFe$_2$O$_4$. The only parameters left to vary were the Debye−Waller factors and the occupation of (B) sites x_B(Ni^{2+}), that is, the inversion parameter i.

A degree of inversion of 1 corresponding to a totally inverted spinel structure was obtained by fitting the EXAFS oscillations at both Fe and Ni edges of the AFeNi_750_20h and AFeNi_900 aerogels, as already found for commercial NiFe$_2$O$_4$. Debye−Waller factors of AFeNi_900 are slightly lower than those of AFeNi_750_20h, in agreement with the higher crystallinity of the aerogels calcined at 900 °C compare to the ones calcined at 750 °C for 20 h.

A slightly different approach was used for the fitting of the sample calcined at 750 °C for 1 h, as a reasonable fit could not be obtained in the same way used for AFeNi_750_20h and AFeNi_900. Qualitative analysis of EXAFS and XANES suggested that AFeNi_750_1h is in an intermediate stage between AFeNi_450 and AFeNi_750_20h. Therefore, AFeNi_750_1h was simulated by a linear combination of the spectra of the AFeNi_450 and AFeNi_750_20h aerogels at both the Fe and Ni edge. To perform this fitting, the program LINCOM,[44] which runs a least-squares routine to minimize the difference between one EXAFS spectrum and the combination of up to nine others, was used in the range 2.5−12 Å^{-1}. The results of the linear combination are shown in Figure 5.

The results of the fitting are quite good at both Fe (R-factor $= 2\%$) and Ni edge (R-factor $= 3\%$). The results of the fitting

TABLE 2: Interatomic Distances (R), Coordination Numbers (N) and Debye−Waller Factors (σ) Obtained by Fitting the Experimental EXAFS spectra of Ni₃Si₂O₅(OH)₄, ANi_450, AFeNi_ae and AFeNi_450 at the Ni K-edge

| | Ni K-edge | | | | | | | | | | | |
| | Ni₃Si₂O₅(OH)₄ | | | ANi_450 | | | AFeNi_ae | | | AFeNi_450 | | |
atom	R (Å)	N	$2\sigma^2$	R (Å)	N	$2\sigma^2$	R (Å)	N	$2\sigma^2$	R (Å)	N	$2\sigma^2$
O	2.07(1)	6	0.017(1)	2.07(1)	6	0.018(1)	2.08(1)	6	0.019(2)	2.08(1)	6	0.030(1)
Ni	3.07(1)	6	0.017(1)	3.07(1)	6	0.018(1)	3.07(1)	6	0.018(1)	3.07(1)	6	0.033(1)
Si	3.26(1)	4	0.014(3)	3.26(2)	4	0.012(2)	3.26(2)	4	0.026(5)	3.26(1)	4	0.013(3)
	R-factor = 24%			*R*-factor = 23%			*R*-factor = 33%			*R*-factor = 28%		
	*R-factor = 18%			**R*-factor = 15%			**R*-factor = 26%			**R*-factor = 20%		

TABLE 3: Interatomic Distances (R), Coordination Numbers (N) and Debye−Waller Factors (σ) Obtained by Fitting the Experimental EXAFS Spectra of AFeNi_ae and AFeNi_450 at the Fe K-edge

| | Fe K-edge | | | | | |
| | AFeNi_ae | | | AFeNi_450 | | |
	R (Å)	N	$2\sigma^2$	R (Å)	N	$2\sigma^2$
O	1.95(1)	5.1	0.033(2)	1.95(1)	5.1	0.028(2)
Fe	2.87(2)	0.8	0.016(2)	2.87(1)	0.8	0.016(3)
Fe	3.04(1)	2.4	0.018(1)	3.04(1)	2.4	0.019(2)
Fe	3.42(4)	1.5	0.032(2)	3.42(2)	1.5	0.024(1)
	R-factor = 39%			*R*-factor = 22%		

at the Fe edge (Figure 5A) are consistent with the sample containing around 35% of AFeNi_450 (ferrihydrite) and 65% of AFeNi_750_20h (nickel ferrite), whereas at the Ni edge (Figure 5B) the fit gives 31% of AFeNi_450 and 69% of AFeNi_750_20h (nickel ferrite), associated errors being about 10%.

IV. Discussion

XRD patterns of the ANi_450, AFeNi_ae, and AFeNi_450 nanocomposites present weak and broad peaks that correspond to those of the reference compound Ni₃Si₂O₅(OH)₄, a nickel phyllosilicates hydroxide. However, the poor crystallinity and low percentage of the nanoparticles in the silica matrix and the presence of the background due to matrix in the aerogels make the phase attribution debatable. Moreover, the nickel hydroxide phase, Ni(OH)₂, which has a similar layered structure as that of nickel silicate hydroxide, presents broad peaks at the same angular values.[45,46] Therefore, the attribution of the phases present in the nanocomposites aerogels just after supercritical drying and after thermal treatment up to 450 °C cannot be unambiguously obtained by conventional XRD. To identify the phases present, local and selective techniques, EXAFS and XANES, were used.

Analysis of both EXAFS and XANES at the Ni edge clearly show that Ni₃Si₂O₅(OH)₄ is the phase present in the aerogel containing only nickel ANi_450 and also in the aerogels containing both iron and nickel, AFeNi_ae and AFeNi_450. Moreover, analysis of EXAFS and XANES at the Fe edge shows that ferrihydrite, a phase very difficult to detect by XRD diffraction due to the poor crystallinity accompanied by low concentration, is also present in AFeNi_ae and AFeNi_450. Therefore, in the aerogels after extraction and up to calcination at 450 °C, iron and nickel are present in two separated phases, ferriydrite and nickel silicate hydroxide. Upon heat treatment at 750 °C for 1 h, the two separate phases of iron and nickel are partially converted into nanocrystalline nickel ferrite. A complete conversion is obtained as the heating at 750 °C is extended up to 20 h or increased up to 900 °C.

A very similar evolution with calcination was recently observed by X-ray absorption spectroscopy on cobalt[22] and

manganese[47] spinel ferrites aerogels prepared with an analogous sol−gel procedure. Two separate phases, one contaning iron in form of ferrihydrite and another one containing either cobalt or manganese were identified in the first stages of heat treatment that evolve to the corresponding Co or Mn ferrites after calcination at high temperature.

The XRD pattern of commercial NiFe₂O₄ contain some unidentified peaks, indicating the presence of some impurities. This observation can explain the high R values obtained by fitting the EXAFS oscillations of commercial NiFe₂O₄ using the parameters of pure NiFe₂O₄. Much lower R values were obtained by fitting the aerogels calcined at 750 °C for 20 h and at 900 °C by using the same parameters.

The inversion parameter i, which indicates the fraction of bivalent cations in octahedral sites, was left to vary in the fitting of commercial NiFe₂O₄ and in the fitting of aerogels containing NiFe₂O₄ (i.e., those calcined at 750 °C for 20 h and at 900 °C).

The structure of stoichiometric NiFe₂O₄, belonging to space group *Fd3m*, is a typical spinel, which means that the cubic unit cell contains 32 oxygens in a close packed cubic arrangement with 24 cations occupying 8 of the 64 available tetrahedral sites and 16 of the 32 available octahedral sites.[48] In a *normal* spinel structure, the 8 tetrahedral sites are occupied by bivalent cations, and the 16 octahedral sites are occupied by trivalent cations. On the other hand, in an *inverse* spinel structure the 8 tetrahedral sites are occupied by trivalent cations, 8 octahedral sites are occupied by trivalent cations, and 8 octahedral sites are occupied by 8 bivalent cations.[49] If the bivalent cations are present on both tetrahedral and octahedral sites the spinel is *partially inverted*. The structural formula for a generic spinel compound MFe₂O₄ can be written as:[50]

$$[M_{1-i}Fe_i]^A[M_iFe_{(2-i)}]^BO_4 \qquad (2)$$

where the amounts in brackets represent the average occupancy of A-sites (tetrahedral) and B-sites (octahedral), and i is the inversion parameter. For a normal spinel $i = 0$, and for an inverted spinel $i = 1$.

Bulk NiFe₂O₄ has a totally inverted spinel structure where all the Ni²⁺ ions occupy octahedral sites and the Fe³⁺ ions are equally distributed between tetrahedral and octahedral sites. However, there are reports in literature that show a different cation distribution between bulk and nanosized ferrites. A mixed spinel structure in which part of Ni²⁺ occupy tetrahedral sites has been suggested for NiFe₂O₄ nanoparticles (10 nm) prepared by high-energy ball milling on the basis of Mössbauer spectroscopy and qualitative EXAFS analysis.[9] In a similar study on slightly smaller NiFe₂O₄ nanoparticles (3−4 nm) prepared by hydrolysis in polyol medium,[51] it is estimated that 10% of Ni²⁺ occupy tetrahedral sites and 90% occupy octahedral sites. However, Nilsen et al. reported that the inverse structure of bulk NiFe₂O₄ is preserved at nanometer scale on NiFe₂O₄ nanoparticles (∼ 40 nm) synthesized in near-critical and supercritical

NiFe$_2$O$_4$ Nanoparticles in an Aerogel Silica Matrix

J. Phys. Chem. C, Vol. 112, No. 40, 2008 **15629**

TABLE 4: Interatomic Distances (R), Coordination Numbers (N), Debye−Waller Factors (σ), and Fractions of Cations in Sites A (x$_A$) and x$_B$ (x$_B$)^a

	Fe K-edge							Ni K-edge					
	AFeNi_750_20 h			AFeNi_900				AFeNi_750_20 h			AFeNi_900		
	R (Å)	N	2σ²	R (Å)	N	2σ²		R (Å)	N	2σ²	R (Å)	N	2σ²
x$_B$ = 0.50(3)							x$_B$ = 1.00(2)						
O	2.04(1)	6.0	0.016(2)	2.04(1)	6.0	0.015(1)	O	2.04(1)	6.0	0.014(1)	2.04(1)	6.0	0.014(1)
Fe	2.95(1)	6.0	0.034(3)	2.95(1)	6.0	0.023(1)	Ni	2.94(1)	6.0	0.024(1)	2.94(1)	6.0	0.018(2)
Fe	3.46(1)	6.0	0.028(4)	3.46(1)	6.0	0.021(1)	Ni	3.46(1)	6.0	0.024(1)	3.46(1)	6.0	0.018(2)
O	3.52(6)	2.0	0.042(3)	3.52(5)	2.0	0.036(2)	O	3.52(4)	2.0	0.014(1)	3.52(4)	2.0	0.020(2)
O	3.64(2)	6.0	0.030(8)	3.64(2)	6.0	0.031(1)	O	3.64(2)	6.0	0.030(5)	3.64(2)	6.0	0.018(4)
x$_A$ = 0.50(3)													
O	1.89(1)	4.0	0.010(1)	1.89(1)	4.0	0.010(1)							
Fe	3.46(1)	12.0	0.028(1)	3.46(1)	12.0	0.021(5)							
O	3.47(2)	12.0	0.040(6)	3.47(2)	12.0	0.040(2)							
Fe	3.61(2)	4.0	0.031(6)	3.61(3)	4.0	0.021(4)							
	R-factor = 36%			R-factor = 33%				R-factor = 30%			R-factor = 34%		
	*R-factor = 32%			*R-factor = 25%				*R-factor = 27%			*R-factor = 25%		

^{a} Obtained by fitting the experimental EXAFS spectra of AFeNi_750_20h and AFeNi_900 at the Fe and Ni K-edge.
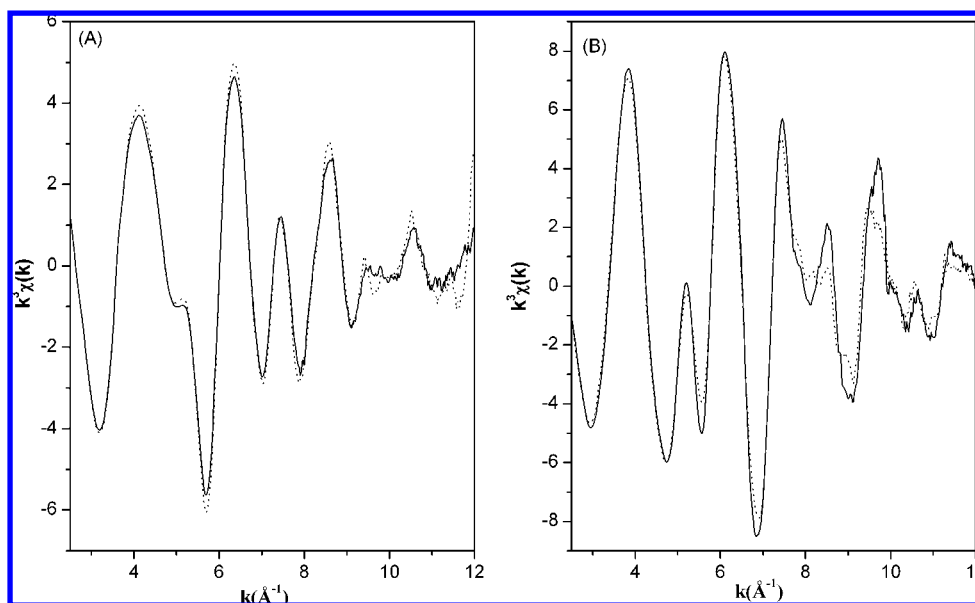

Figure 5. $k^3\chi(k)$ spectra of the (A) Fe edge and (B) Ni K-edge for AFeNi_750_1h from experiment (—) and linear combination (···) of the spectra AFeNi_450 and AFeNi_750_20h aerogels.

water.[52] Therefore, the cation distribution of nanosized nickel ferrite is controversial, and the way different synthetic routes can affect the degree of inversion is still a matter of debate.

In this work, a quantitative analysis of the degree of inversion of commercial bulk NiFe$_2$O$_4$ and of nanocomposite NiFe$_2$O$_4$−SiO$_2$ aerogels at both Fe and Ni K-edge was performed by fitting the EXAFS oscillations curves. The inversion parameter i was refined during the fitting, along with the Debye−Waller factors. By fitting i, an accurate determination of the percentage of occupancy of tetrahedral (A) and octahedral (B) sites by Fe^{3+} and Ni^{2+} was achieved.

The fitting of the EXAFS oscillations of the aerogels AFeNi_900 and AFeNi_750_20h gave an inversion degree of 1. According to eq 2, the value of $i = 1$ means that 100% of Ni^{2+} occupies octahedral sites, whereas 50% of Fe^{3+} occupies tetrahedral sites and 50% occupies octahedral sites. Interestingly, the inversion degree obtained for the NiFe$_2$O$_4$ nanoparticles corresponds to that of bulk NiFe$_2$O$_4$. This is in agreement with our previous work on cobalt[22] and manganese[47] ferrite nanocomposites aerogels, whose inversion degree were found to be

similar to the values of the corresponding bulk materials ($i = 0.7$ and 0.2, respectively).

V. Conclusions

The evolution of the structure of a series of NiFe$_2$O$_4$−SiO$_2$ nanocomposites aerogels as a function of the calcination temperature was investigated by analyzing the local environment around Fe and Ni cations using X-ray absorption spectroscopy. The aerogels after supercritical drying and after calcination up to 450 °C contain two separate phases dispersed in the amorphous silica matrix: ferrihydrite and a nickel silicate hydroxide. Further heat treatment promotes the formation of the nickel ferrite, which is complete after calcination at 750 °C for 20 h, or alternatively after calcination at 900 °C for 1 h. XANES analysis was used to determine the oxidation state of iron and nickel ions, which was found to be +3 and +2, respectively, in all samples. The relative distribution of Fe^{3+} and Ni^{2+} ions between octahedral and tetrahedral sites for commercial bulk NiFe$_2$O$_4$ and for AFeNi_750_20h and AFe-

Carta et al.

Ni_900 was determined by fitting of EXAFS data. A totally inverted spinel structure, where all Ni^{2+} occupies octahedral sites and Fe^{3+} cations are equally distributed between tetrahedral and octahedral sites, was obtained for both bulk and nanocrystalline $NiFe_2O_4$.

References and Notes

(1) Han, D. H.; Luo, H. L.; Yang, Z. *J. Magn. Magn. Mater.* **1996**, *161*, 376.

(2) Tae-Jong, Y.; Jun Sung, K.; Byung Geol, K.; Kyeong Nam, Y.; Myung-Haing, C.; Jin-Kyu, L. *Angew. Chem., Int. Ed.* **2005**, *44*, 1068.

(3) Giri, A. K.; Pellerin, K.; Pongsaksawad, W.; Sorescu, M.; Majetich, S. A. *IEEE Trans. Magn.* **2000**, *36*, 3029.

(4) Singhal, S.; Chandra, K. *J. Solid State Chem.* **2007**, *180*, 296.

(5) Shultz, M. D.; Calvin, S.; Fatouros, P. P.; Morrison, S. A.; Carpenter, E. E. *J. Magn. Magn. Mater.* **2007**, *311*, 464.

(6) Zhao, Z.; Zheng, Z.; Wong, K. W.; Wang, S.; Huang, B.; Li, D. *Electrochem. Commun.* **2007**, *9*, 2606.

(7) Baruwati, B.; Guin, D.; Manorama, S. V. *Org. Lett.* **2007**, *9*, 26–5377.

(8) Cote, L. J.; Teja, A. S.; Wilkinson, A. P.; Zhang, Z. J. *Fluid Phase Equilib.* **2003**, *210*, 307.

(9) Chinnasamy, C. N.; Narayanasamy, A.; Ponpandian, N.; Chatto-padhyay, K.; Shinoda, K.; Jeyadevan, B.; Tohji, K.; Nakatsuka, K.; Furubayashi, T.; Nakatani, I. *Phys. Rev. B,* **2001**, *63*, 184108.

(10) Morrison, A. H.; Haneda, K. *J. Appl. Phys.* **1981**, *52*, 2496.

(11) Ramalho, M. A. F.; Gama, L.; Antonio, S. G.; Paiva-Santos, C. O.; Miola, E. J.; Kiminami, R. H. G. A.; Costa, A. C. F. M. *J. Mater. Sci.* **2007**, *42*, 3603.

(12) Misra, R. K. D.; Gubbala, S.; Kale, A.; Egelhoff Jr, W. F *Mater. Sci. Eng., B* **2004**, *111*, 164.

(13) Li, L.; Li, G., Jr.; Inomata, H. *Chem. Mater.* **2000**, *12*, 3705.

(14) George, M.; John, A. M.; Nair, S. S.; Joy, P. A.; Anantharaman, M. R. *J. Magn. Magn. Mater.* **2006**, *302*, 190.

(15) Da Silva, J. B.; Mohallem, N. D. S. *J. Magn. Magn. Mater.* **2001**, *226*, 1393.

(16) Montemayor, S. M.; García-Cerda, L. A.; Torres-Lubián, J. R.; Rodríguez-Fernández, O. S. *J. Sol-Gel Sci. Techn.* **2007**, *42*, 181.

(17) Moscovici, J.; Michalowicz, A.; Decker, S.; Lagadic, I.; Latreche, K.; Klabunde, K. *J. Synchrotron Rad.* **1999**, *6*, 604.

(18) Moscovici, J.; Benzakour, M.; Decker, S.; Carnes, C.; Klabunde, K.; Michalowicz, A. *J. Synchrotron Rad.* **2001**, *8*, 925.

(19) Carta, D.; Corrias, A.; Mountjoy, G.; Navarra, G. *J. Non-Cryst. Solids* **2007**, *353*, 1785.

(20) Corrias, A.; Mountjoy, G.; Piccaluga, G.; Solinas, S. *J. Phys. Chem. B* **1999**, *103*, 10081.

(21) Carta, D.; Mountjoy, G.; Gass, M.; Navarra, G.; Casula, M. F.; Corrias, A. *J. Chem. Phys.* **2007**, *127*, 204705.

(22) Carta, D.; Mountjoy, G.; Navarra, G.; Casula, M. F.; Loche, D.; Marras, S.; Corrias, A. *J. Phys. Chem. C* **2007**, *111*, 6308.

(23) Corrias, A.; Navarra, G.; Casula, M. F.; Marras, S.; Mountjoy, G. *J. Phys. Chem. B* **2005**, *109*, 13964.

(24) Koningsberger, D. C.; Prins, R. *X-ray Absorption. Principles, Applications, Techniques of EXAFS, SEXAFS and XANES*; Wiley: New York, 1988.

(25) Nakagawa, M.; Yuya, T.; Tachibana, Y.; Takada, H.; Nitani, S.; Emura, T.; Yamamoto, A. *J. Magn. Magn. Mater.* **2005**, *288*, 366.

(26) Harris, V. G.; Koon, N. C.; Williams, C. M.; Zhang, Q.; Abe, M.; Kirkland, J. P. *Appl. Phys. Lett.* **1996**, *68*, 15.

(27) Chinnasamy, C. N.; Yang, A.; Yoon, S. D.; Hsu, K.; Schultz, M. D.; Carpenter, E. E.; Mukerjee, S.; Vittoria, C.; Harris, V. G *J. Appl. Phys.* **2007**, *101*, 09M509.

(28) Zhang, J.; Wang, Z. L.; Chakoumakos, C.; Yin, J. S. *J. Am. Chem. Soc.* **1998**, *120*, 1800.

(29) Wang, J; Wu, Y.J.; Zhu, Y. J. *Int. J. Mod. Phys. B* **2007**, *21* (5), 723.

(30) Lee, J.-G; Park, J. Y.; Kim, C. S. *J. Mater. Sci.* **1998**, *33*, 3965.

(31) Decarreau, A. *Bull. Minéral.* **1980**, *103*, 579.

(32) Klementiev, K. V. *Appl. Phys.* **2001**, *34*, 209.

(33) Tomic, S.; Searle, B.G. Wander, A.; Harrison, N. M.; Dent, A. J.; Mosselmans, J. F. W.; Inglesfield, J. E. *CCLRC Technical Report DL-TR-2005−001, ISSN 1362−0207*; CCRLC: Warrington, UK, 2004.

(34) Gurman, S. J.; Binsted, N.; Ross, I. *J. Phys. C* **1984**, *17*, 143.

(35) Von Barth, U.; Hedin, L *J. Phys. C* **1972**, *5*, 1629.

(36) Crozier, E. D. *Nucl. Instr. Method Phys. Res. B* **1997**, *133*, 134.

(37) EXCURV98 Manual (http://srs.dl.ac.uk/XRS/Computing/Programs/excurv97/excurv98guide.htm)

(38) Error Report of the International XAFS Society Standards and Criteria Committee, (http://ixs.iit.edu/subcommitteereports/sc/) 2000.

(39) Bianconi,A. In *X-ray Absorption: Principles, Applications, Techniques of EXAFS, SEXAFS and XANES*; Koninbsberger, D. C. Prins, R., Eds; Wiley: New York, 1988; *Ch. 11*.

(40) PDF Card 22−0754.

(41) PDF Card 10−325.

(42) Subramanyam, K. N. *J. Phys. C* **1971**, *4*, 2266.

(43) Scheinost, A. C.; Sparks, D. L. *J. Colloid Interface Sci.* **2000**, *223*, 167.

(44) *LINCOM, Linear combination program from CCP3, Collaborative Computational Project 3*; Daresbury Laboratory: U.K.

(45) Manceau, A.; Schlegel, M.; Nagy, K. L.; Charlet, L. *J. Colloid Interface Sci.* **1999**, *220*, 181.

(46) Scheinost, A. C.; Sparks, D. L. *J. Colloid Interface Sci.* **2000**, *223*, 167.

(47) Carta, D.; Casula, M. F.; Mountjoy, G.; Corrias, A. *Phys. Chem. Chem. Phys.* , DOI: 10.1039/b800359a.

(48) Sickafus, K. E.; Wills, J. M. *J. Am. Ceram. Soc.* **1999**, *82*, 12–3279.

(49) Harris, V. G.; Koon, N. C.; Williams, C. M.; Zhang, Q.; Abe, M.; Kirkland, J. P. *Appl. Phys. Lett.* **1996**, *68*, 15.

(50) Zhang, Z. J.; Wang, Z. L.; Chakoumakos, B. C.; Yin, J. S. *J. Am. Chem. Soc.* **1998**, *120*, 1800.

(51) Chkoundali, S.; Ammar, S.; Jouini, N.; Fiévet, F.; Molinié, P.; Danot, M.; Villain, F.; Grenèche, J-M *J. Phys.: Condens. Matter* **2004**, *16*, 4357.

(52) Nilsen, M. H.; Nordhei, C.; Ramstad, A. L.; Nicholson, D. G.; Poliakoff, M.; Cabañas, A. *J. Phy.Chem.C.* **2007**, *111*, 6252.

JP803982K